The Role of 3D Subsurface Modelling for Geotechnical Engineering Data Visualization

Urooba Farman Tanoli[1], Muhammad Usman Azhar[1*], Tofeeq Ahmad[2], Muhammad Shahid Khawaja[3], and Muneeb Ahmed[1]

[1]*"Department of Earth Sciences, The University of Haripur, Khyber Pakhtunkhwa, Pakistan"*
[2]*"United Arab Emirates University, Al Ain, Abu Dhabi, United Arab Emirates"*
[3]*"Emaan Engineering SMC Private Limited, Wah Cantt, Pakistan"*
*Corresponding author: musmanazhar@uoh.edu.pk"

Abstract

The main objective of this study is to explore the application of 3D subsurface modelling as an advanced data visualization technique in geotechnical engineering prior to the designing and planning of civil engineering infrastructure. A detailed three-dimensional subsurface model of New City Phase-II, Wah Cantt, is created using a large dataset of bore logs, encompassing coordinates, depth measurements, elevation data, and lithology types of the study area. The combination of Geographic Information System (GIS) and Computer-Aided Design (CAD) technology has simplified the creation of this comprehensive three- dimensional model, resulting in a considerable advancement in the representation of complicated subsurface formations. The subsurface model highlighted the spatial distribution and lithological features of subsurface layers, indicating the presence of silty clay with varied stiffness at different depths. The validation using field data suggested a substantial spatial correlation, demonstrating the model's reliability. This study emphasizes the importance of 3D subsurface modelling in improving geotechnical site characterization, foundation design, hazard risk assessment, and effective land use planning. Future research will employ advanced imaging technologies, and data integration approaches to increase model accuracy and feasibility in a variety of geotechnical contexts.

Keywords: 3D subsurface modelling, borehole logs, geographic information systems, geotechnical investigations, data visualization, foundation design

1. Introduction

Traditionally, the geotechnical analysis, designing, and planning for subsurface engineering projects such as buildings, foundations, roads, and tunnels relied on manual design techniques. These methods, however crucial, were time-consuming and labor-intensive. Over the last few decades, the advancement of Geographic Information System (GIS) and Computer-Aided Design (CAD) technologies have revolutionized this field. These innovations provide comprehensive 3D capabilities, considerably enhancing the visual representation and interpretation of subsurface data. Thereby, improving the efficiency and accuracy of creating three-dimensional (3D) solid models that identify the lithology and pertinent soil properties at a specific site using a variety of geotechnical data and modelling tools.

Throughout the last three decades, several researchers have presented a variety of modelling theories and techniques to construct three-dimensional solid models of subsurface using diverse kinds of geological and geotechnical data (borehole data, geological maps, geotechnical survey records, cross-sections, structural information, etc.). Countless attempts at 3D modelling of geotechnical and geological characteristics have been performed to date (De Rienzo et al., 2008; Royse et al., 2009; Tame et al., 2013; Touch et al., 2014). Geologists are nowadays capable of building 3D spatial models from subsurface layers in the urban sector to predict soil properties and reduce the risks and ambiguity associated with urban planning. These capabilities are made possible by more sophisticated computational tools, modern geodatabases, and advancements in computational speed and performance,

acquisition, and digitalization of geological data (Kessler et al., 2009; De Beer et al., 2012a, b; Abuzar et al., 2018).

In the case of geological and geotechnical engineering, a detailed understanding and accurate mapping of the subsurface geology is crucial for designing underground engineering structures such as foundations for buildings, roads, and tunnels. Geotechnical engineers construct and attribute 3D geological subsurface models in two stages: by creating a 3D geological framework model and then attributing this model with appropriate geotechnical characteristics (Kessler et al., 2009). Various methodologies, such as "geotechnical baseline methods" (Staveren and Knoeff, 2004), probability studies, and Monte Carlo simulations (Eivind and Holden, 1994; Viseur and Shtuka, 1997) are being utilized to estimate the potential errors that might arise in the design of an engineering structure due to the lack of information concerning the parameters of the subsurface.

Several ways for producing 3D solid models generated from an array of geotechnical data types have been developed and deployed within a GIS framework (Lemon and Jones, 2003; Kaufmann and Martin, 2009; Ming et al., 2010; Zhu et al., 2012; Ghiglieri et al., 2016). Boreholes are the most used data source in subsurface modelling because they are simple, intuitive, accurate, and detailed for practical users. Several modelling approaches have been suggested and used, including the development of discrete stratigraphic layers utilizing surfaces interpolated from borehole data control points and the simultaneous blending of these units into an individual solid model (Gallerini and De Donatis, 2009; Akiska et al., 2013).

Utilizing such vague subsurface information, however, gives rise to great difficulty. The data is often complex to access, abundant, heterogeneous and has inherent uncertainties. These methods, as discussed earlier, offer their advantages and limitations based on the use of interpolation techniques and the capacity to represent missing and discontinuous surfaces in three dimensions. However, reliable reconstruction of complex 3D subsurface structures from discrete geotechnical data tends to be a real challenge. This paper investigates subsurface mapping techniques to develop a three-dimensional (3D) subsurface model, aiming to enhance the preliminary design process, improve hazard identification, and planning of soil investigations for shallow foundations.

2. Study Area

The study area is located in New City Phase-II, Wah Cantt, near Taxila, northwest of Islamabad (Punjab, Pakistan). It lies between 33.74ºN latitudes and 72.72ºE longitudes, and its elevation is roughly 452m (1483 ft). The area extends about 4.43 km2 and is easily accessible via the M1 motorway near the Brahma Jhang Bahtar Interchange (Figure 1). The region is located in the MBT foothills, where Quaternary deposits overlie the Murree Formation of the lower Miocene (Sheikh et al., 2008). All the boreholes are drilled in quaternary deposits for the shallow foundation.

3. Materials and Methods

Three core steps are usually found in any 3D modelling workflow, as shown in Figure 2. These steps involve data compilation and structuring, the 3D modelling process and uncertainty or accuracy assessment depending upon the type of data used (Turner, 2003; Kauffman and Martin, 2008; Caumon et al., 2009). This stage can be completed using any database and modelling software capable of 3D visualization. The detailed methodology adopted in this study is as follows:

3.1. Data Compilation/Preparation Stage

A total of 58 boreholes drilled up to 7.62m (25ft) depth in the project area were finalized as the primary data source, covering an area of approximately 4.43 km2 (Figure 3). The groundwater table (GWT) was not encountered in any boreholes down to the maximum depth explored. The raw data of borehole logs in .xls (Excel sheet) format consisted of several columns providing comprehensive information about depth, sample number, description of soil strata, SPT blows, and SPT-N values.
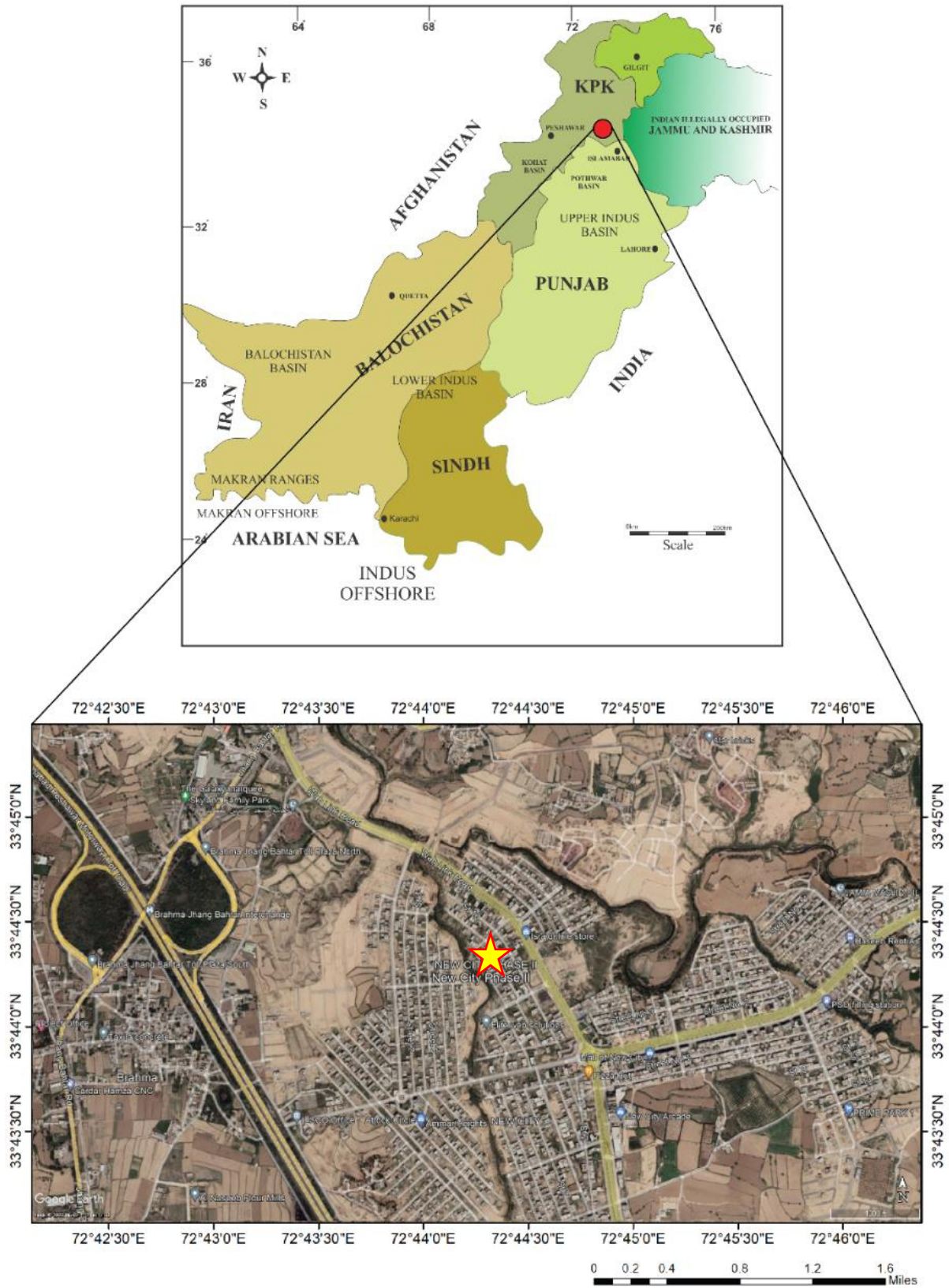
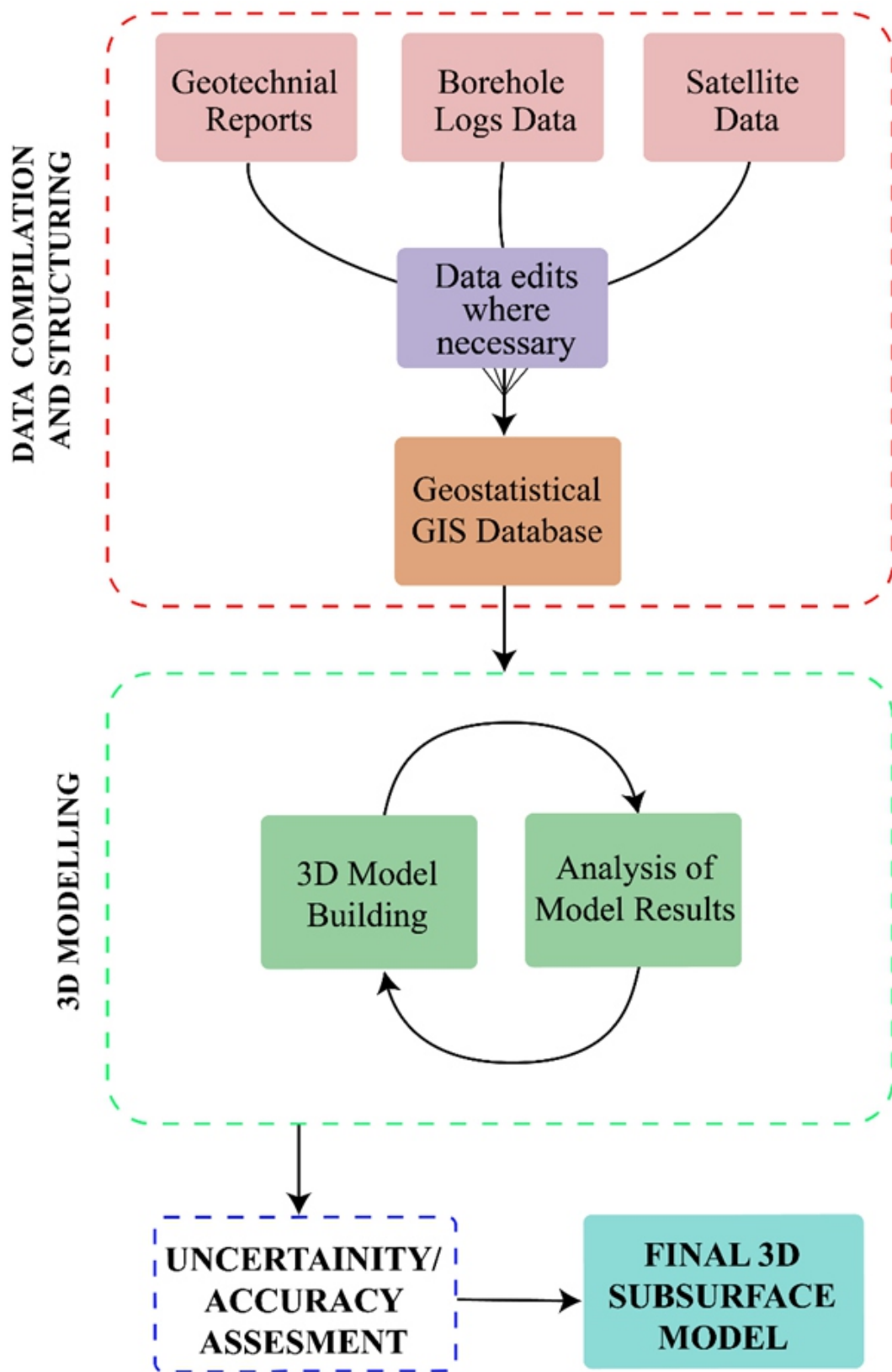Fig. 1. Location of Study Area (Google Earth, August 2022)

Fig. 2. 3D Modelling workflow of the study area (modified from Turner, 2006; Kauffman and Martin, 2008; Caumon et al., 2009)
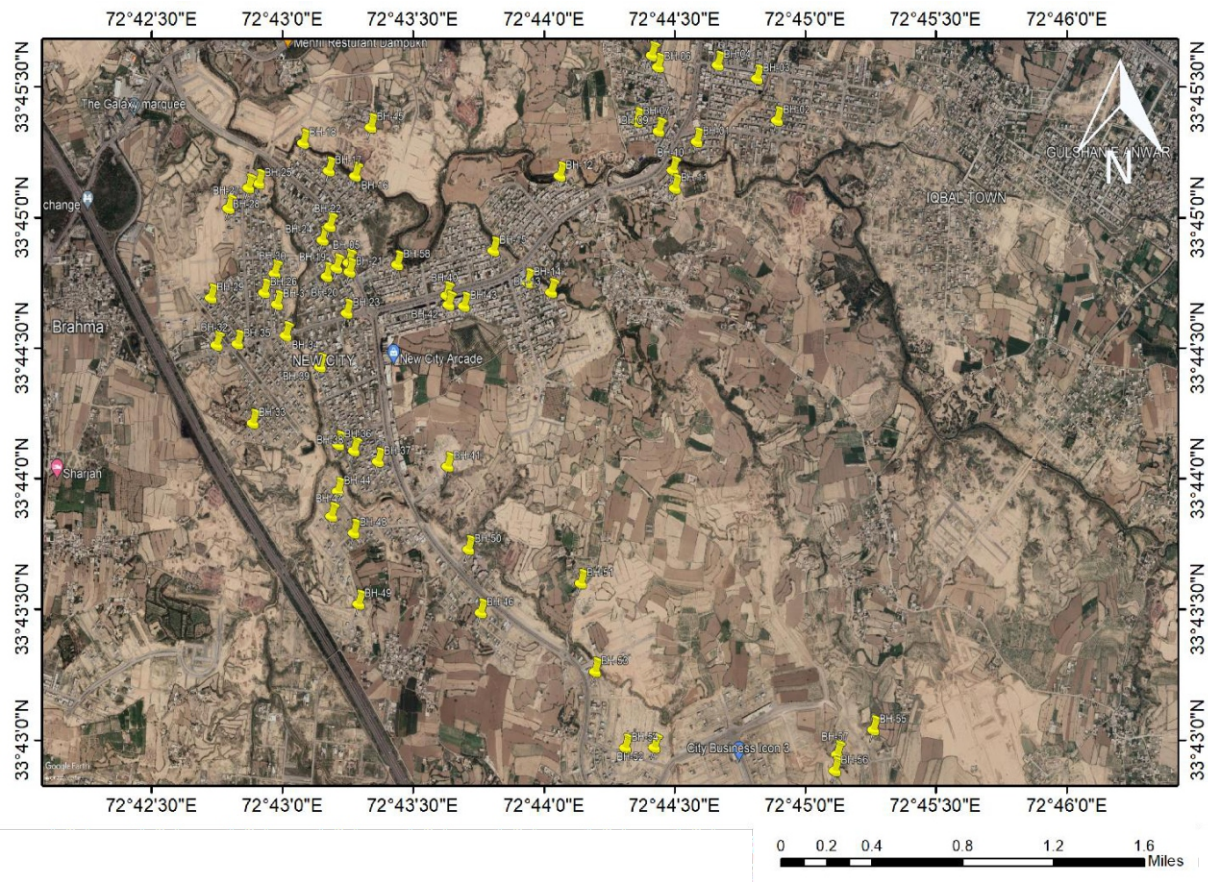
Fig. 3. Data Points and sitemap of the study area (Google Earth, August 2022)

A 3D modelling process requires an effective interpolation method and visualization software. The selection criteria for software determination must depend on the software's capabilities and available resources. RockWare's RockWorks16, a versatile 3D geomodelling software, was used in this study. The RockWorks software package is a sophisticated tool for managing, analyzing, and visualizing geological data.

In order to make lithological data compatible with RockWorks, it was necessary to transform the data into a template specified in RockWork's manual. The lithological data was then manually entered into the Excel sheets. Each lithology type was assigned a G-value, a unique number that the program substitutes for the material type while making a model. A total of 3 sheets were prepared in a single Excel file naming location, lithology, and lithology type. The location sheet included information related to Borehole Name, Easting, Northing,

Elevation and Total Depth values of all the boreholes. The lithology sheet stored depth from top to bottom and lithologic unit names. The lithology type sheet was, however, optional, but it saved time from doing some basic settings (pattern, size, background, foreground value, etc) manually again and again (Appendix-A, -B, -C).

3.2. Project Set Up

Before modelling, a project setup was needed to define the modelling parameters. The coordinates system was set to be UTM Zone 43, WGS-1984 (NAD-83), and the vertical units were set to meters. After importing the prepared Excel file, the software interpolated all the data in the RockWorks geodatabase. Here, the model dimension in terms of 3D space and resolution had to be defined. For this purpose, all the borehole data was scanned to define model dimensions automatically based on the provided data. The X and Y resolution or node

spacing was set to 15 meters, and the Z resolution to 0.075 meters. This resolution might seem relatively low given the size of the cells; however, the area being modelled was relatively vast. The smaller the cell size, the larger the processing time will be. So, for this study, a Z resolution of 0.075m produces reasonable results while allowing for the quick reprocessing of surfaces. Every surface in this model used this node structure and extent as its spatial boundary.

3.3. 3D Modelling Stage

Once all the lithologic data was validated and completed, 3D modelling began. In RockWorks, numerous algorithms are available for interpolation depending on the data type under consideration. RockWorks offers two algorithms for lithologic solid modelling. The most common algorithm is Horizontal Lithoblending Solid Modelling, in which solid lithology models such as profiles, sections, fences, surface and plan maps, and models are created for display. The solid model voxel nodes are assigned by scanning horizontally from each borehole in search circles with progressively increasing diameters.

Another algorithm for the solid modelling method, Closest Point, sets a voxel node's value equal to that of the closest data point, independent of the node's proximity to the point or the values of its other neighbors. When creating models with non-gradational values, this method is helpful. This approach generates a solid model with sudden node changes, which can be applied to complicated non-stratiform geology, such as multiple intrusions, karst, impact craters, etc., for lithology modelling (Manual, 2013). Within the scope of this research, the "Horizontal Lithoblending" was chosen as the best interpolation algorithm to fulfill the prerequisites of 3D subsurface modelling (Figure 4).

4. Results and Discussions

The classification test results based on the Unified Soil Classification System (USCS) revealed that the top soil strata mainly comprised very stiff to hard silty clay (CL-ML group) and were encountered throughout the

drilling depth. However, the subsoil profiles developed based on borehole logs showed slight variation between these lithologic layers, such as color, texture, presence of trace grassroots, concretions, etc., at varying depths. Based on these variations, the layers were termed Silty Clay-1, Silty Clay-2, and Silty Clay-3, respectively. The detailed interpretation of 3D subsurface models of the study area is as follows:

4.1. Layer Distribution

The 3D subsurface model constructed from the borehole data revealed a distinct stratification of silty clay layers in the study area. The analysis indicated that the thickness of Silty Clay-1 ranges from 0m to 4.57m across the study area. Silty Clay-2 varies in thickness between 0.91m and 6.70m, while Silty Clay-3 exhibits a thickness ranging from 0.91m to 5.18m (Figure 6).

4.2. Lithological Changes

Each silty clay layer exhibited variations in lithology, with SC-1 showing the least amount of lithological diversity, primarily consisting of fine-grained silts. SC-2 displayed more variability with occasional interbedding of coarser materials, indicating a more dynamic depositional environment. SC-3 showed the most complexity in lithology, with significant grain size and mineral composition variations. These gradual lithological changes within each layer suggested a continuous and relatively stable depositional process over time.

4.3. Spatial Variation

Spatially, the distribution of these layers varied across the study area. SC-1 is more prevalent in the northern and central regions, reflecting recent sedimentation processes. SC-2 had a wider distribution, covering most of the study area with higher concentrations in the southern region. SC-3 was more uniformly distributed, but its presence was notably more substantial in the deeper, central parts of the study area. This spatial variation indicated the historical geological processes and sedimentary environments that have influenced the deposition and formation of these layers

(Figure 6).

4.4. Correlation between Layers

The study revealed a consistent correlation between SC-1 and SC-2, with SC-1 usually overlaying SC-2. This relationship suggests a transitional deposition process from one layer to the other. The presence of SC-3 beneath SC-2 in most locations indicated a recurring soil sequence (Figure 4).

4.5. Geotechnical Implications

The composition and arrangement of these silty clay layers have significant geotechnical implications. SC-1, being the uppermost layer, will most directly impact surface-level construction projects, particularly regarding soil stability and drainage. SC-2's intermediate depth and variable lithology could affect the soil's shear strength and compaction properties, which are critical factors in foundation design and slope stability analyses.

With its complex lithology, the deepest layer, SC-3, could influence deeper geotechnical structures or foundations, especially in load-bearing capacity and long-term settlement.

4.6. Geostatistical Analysis

The kriging variogram is a vital geostatistical method used for spatial interpolation and prediction (Ali et al., 2019). By plotting semivariance versus lag distance, the variogram displays the geographic distribution of the data, offering insights into spatial correlation and pattern. It is crucial for understanding the spatial continuity of the studied phenomena and making exact spatial predictions using kriging, an interpolation approach that determines values at unsampled locations using the variogram model. In this study, the Surfer software was used for developing kriging variograms and contour plots for all three layers, demonstrating the variation in layer thickness (Figs. 5, 6).
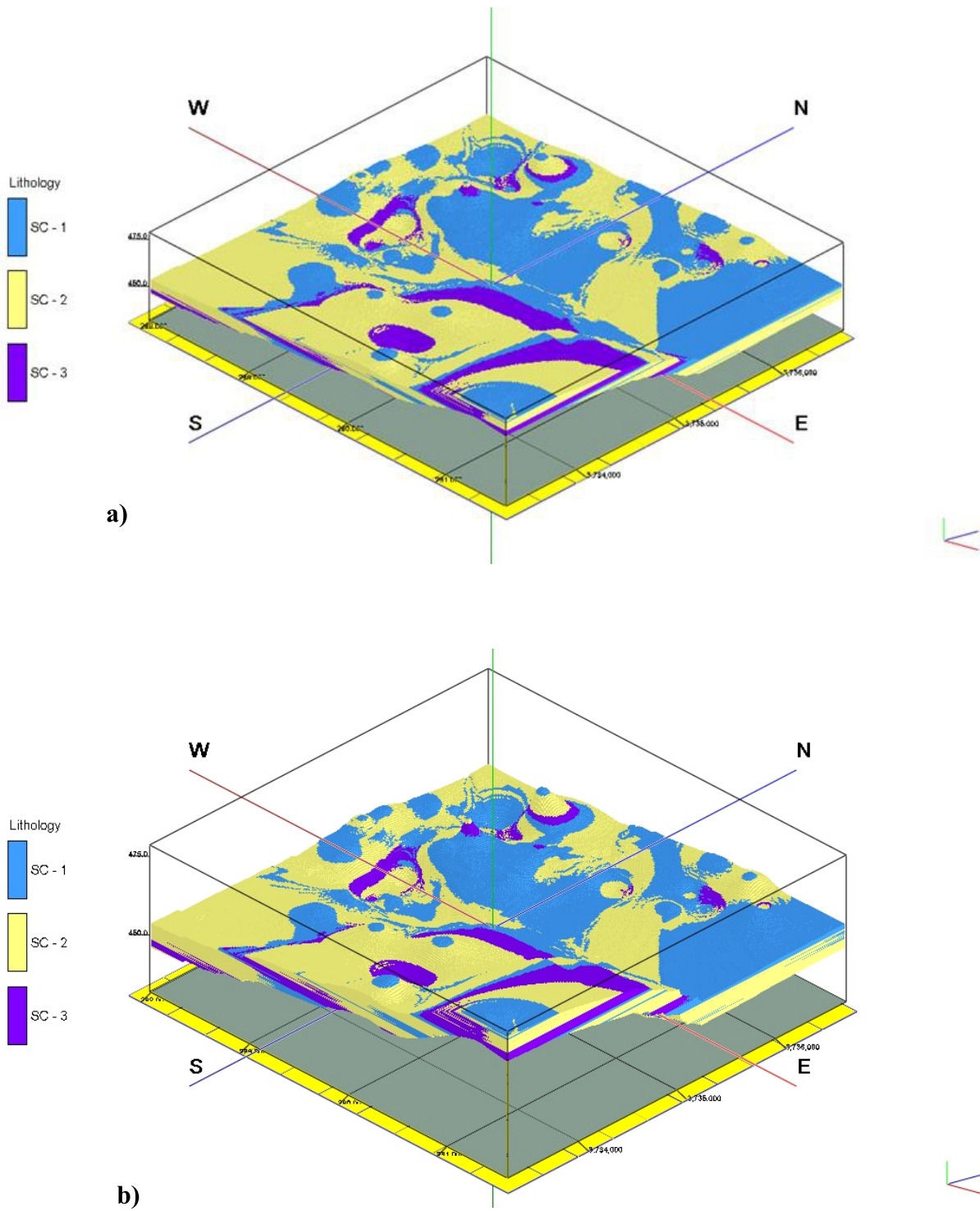
Fig. 4. 3D Subsurface Model of study area created using Horizontal Lithoblending algorithm
a)Vertical Exaggeration:15x b) Vertical Exaggeration:25x
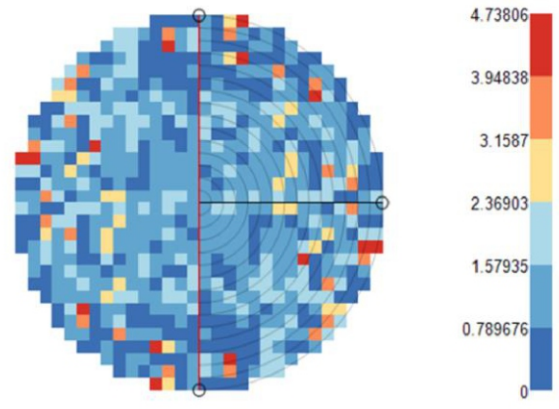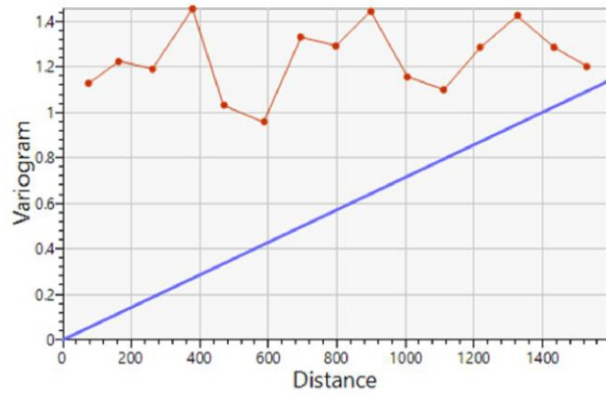
Fig. 5. Illustration of the kriging variograms for all three layers, SC-1, SC-2 and SC-3

Fig. 6. A contour plot illustrating the thickness (meters) and distribution of the
a) SC-1 layer, b) SC-2 layer & c) SC-3 layer

30

4.7. Validation of Model

The validity and accuracy of the 3D subsurface model were assessed by comparing the thickness of three subsurface layers at 12 different points, derived from field observations, with the predicted 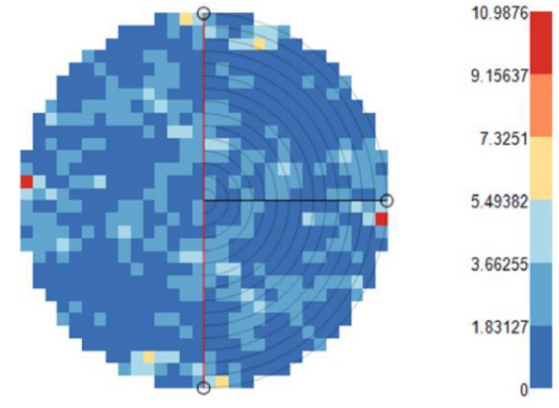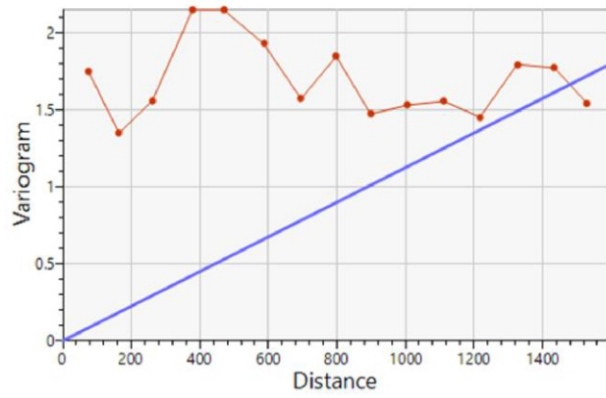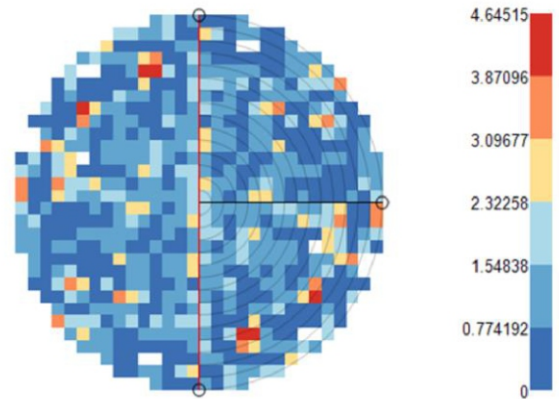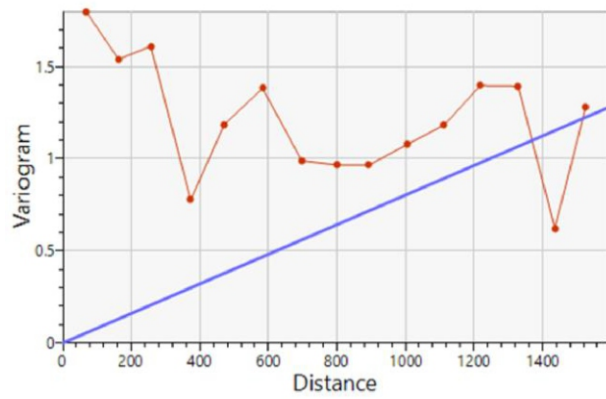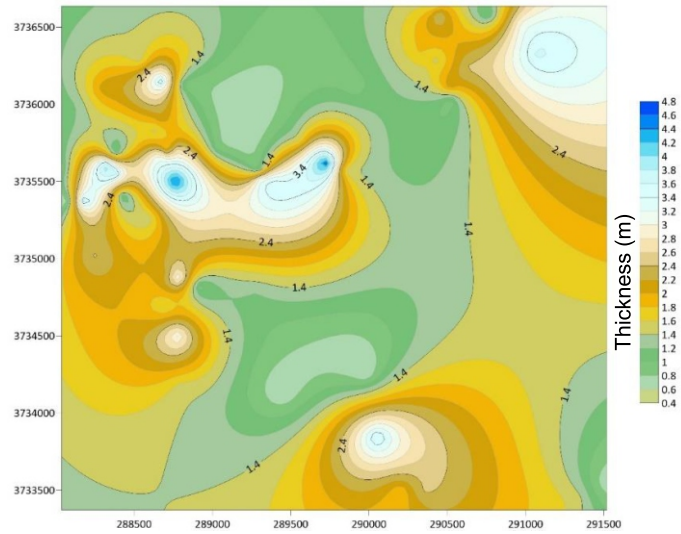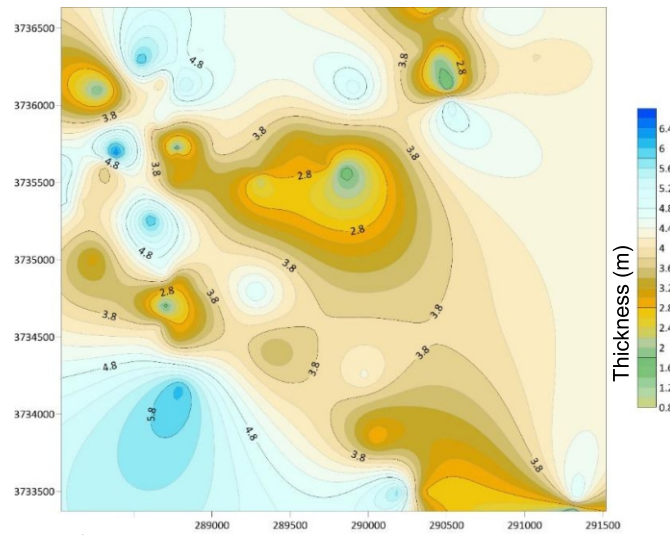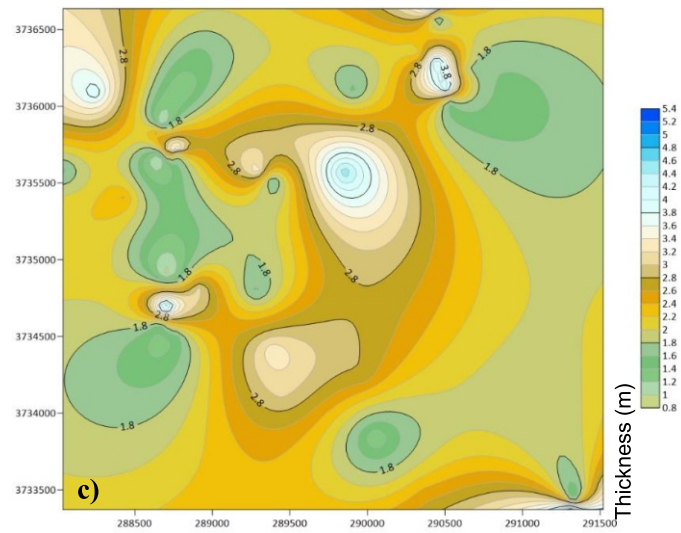thickness values at the corresponding coordinates. Upon plotting a graph of observed versus predicted values, the coefficient of determination (R^2) was calculated to evaluate the model's reliability. The analysis revealed a moderate to high level of reliability in the subsurface model (Figure 7). The coefficient of determination, R^2 (a number between 0 and 1), is a statistical metric quantifying the goodness of fit of a regression model that measures how well the model predicts the outcome. Specifically, it indicates the proportion of variance in the dependent variable (observed thickness of subsurface layers) that is explained by the independent variable (predicted values from the model). The analysis of all three subsurface layers revealed the following R^2 values:

I. The R^2 value for SC-1 was roughly 0.9134, meaning that nearly 91.34% of the variance in the measured thickness can be explained by the model. It implies a high degree of accuracy, with the model accurately estimating the thickness of the underlying layers.

II. The R^2 value of SC-2 was roughly 0.848, suggesting that around 84.8% of the variation in the observed data is accounted for by the model's predictions. Although significantly lower than SC-1, this value still demonstrates good predictive capability.

III. The R^2 value of SC-3 was roughly 0.7304, which is lower than the preceding two values. It implies that the model explains around 73.04% of the variation in the observed data. While this figure shows a modest degree of accuracy, the model nevertheless produces relatively accurate estimates for the thickness of underlying layers.

However, it is necessary to comprehend certain limitations, such as potential data gaps or variability in data quality across multiple boreholes. While these components mentioned above impose some degree of uncertainty, the entire model accurately reflects the available data and appropriately depicts subsurface conditions. Future research might boost the model's accuracy by integrating new data points and applying sophisticated geostatistical techniques for enhanced spatial interpolation.
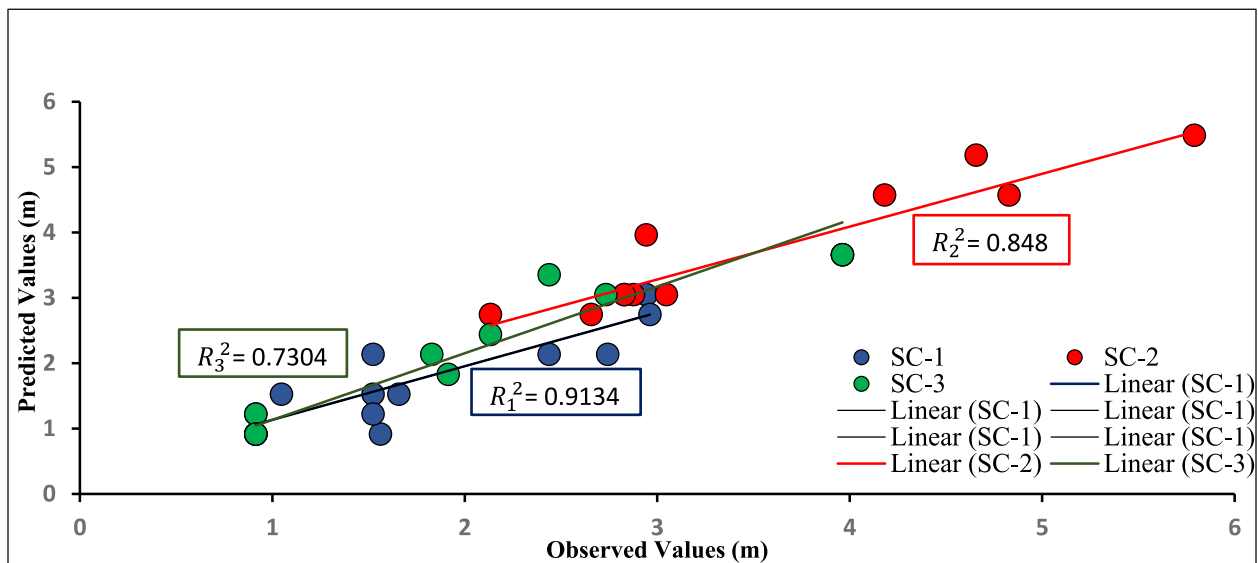

Fig. 7. Coefficient of determination (R^2) of observed versus predicted thickness (m) values of all three subsurface layers: SC-1, SC-2 and SC-3

5. Conclusion

This study used borehole data and geomodelling techniques to create a 3D subsurface model of the New City Phase-II region in Wah Cantt, Pakistan. The model identified three silty clay strata (SC-1, SC-2, and SC-3) of varying thicknesses and spatial distributions within the 4.43 km² research region. The key insights from the 3D modelling are:

I. The variation of SC-1's layer thickness ranged from 0m to 4.57m, SC-2 from 0.91m to 6.70m, and SC-3 from 0.91m to 5.18m.

II. SC-1 was predominant in the northern and central areas, whereas SC-2 had a broader distribution with a higher prevalence in the south. Simultaneously, SC-3 was more evenly distributed but dominant in the deeper, central regions of the study area.

III. The coefficient of determination (R^2) values of all three layers demonstrated moderate to high model reliability with 0.9134 for SC-1, 0.848 for SC-2, and 0.7304 for SC-3.

The study's findings suggest that 3D subsurface models may considerably improve the selection and designing of appropriate subsurface foundation systems, geotechnical risk assessment, and informed decision-making processes in urban development and infrastructure projects. However, several areas still require further research to address current challenges. Future research in 3D subsurface modelling should focus on integrating improved imaging technologies, implementing hybrid modelling strategies, enhancing data visualization techniques, reducing uncertainties, and undertaking various field validation testing.

Authors Contribution

Urooba Farman Tanoli, first author, conducted the analysis, interpretation, and visualization of data, and involved in manuscript's write up. Muhammad Usman Azhar, proposed the main concept, reviewed, and proofread the manuscript. Tofeeq Ahmad, carried out the technical review before submission and provided suggestions for improving the manuscript. Muhammad Shahid Khawaj, facilitated in providing the extensive borehole data used in the study. Muneeb Ahmad, assisted in the interpretation and analysis of the data.

Conflicts of Interest

The authors declare no conflict of interest regarding the publication of this article.

References

Abuzar, M.K., Shakir, U., Ashraf, M.A., Mukhtar, R., Khan, S., Shaista, S., & Pasha, A.R. (2018). GIS based risk modeling of soil erosion under different scenarios of land use change in Simly watershed of Pakistan. *Journal of Himalayan Earth Sciences*, *51*(2), 132-143.

Akiska, S., Sayili, İ.S., Demirela, G. (2013). Three-dimensional subsurface modelling of mineralization: a case study from the Handeresi (Çanakkale, NW Turkey) Pb-Zn-Cu deposit. *Turkish Journal of Earth Sciences* , *22*(4), 574-587. https://doi.org/10.3906/yer-1206-1

Ali, W., Nafees, M,. Turab, S.A., Khan, M.Y., & Rehman, K. (2019). Drinking water quality assessment using water quality index and geostatistical techniques, Mardan District, Khyber Pakhtunkhwa, Pakistan. *Journal of Himalayan Earth Sciences*, *52*(1), 65-85.

Caumon, G., Collon-Drouaillet, P.L.C.D., Le Carlier de Veslud, C., Viseur, S., & Sausse, J. (2009). Surface-based 3D modelling of geological structures. *Mathematical Geosciences*, *41*(8), 927-945. https://doi.org/10.1007/s11004-009

-9244-2

Eivind, D., & Holden, L. (1994). Mixed Reservoir Characterization Methods. *Conference Proceedings at the University of Tulsa Centennial Petroleum Engineering Symposium, Tulsa, Oklahoma, August 1994.* https://doi.org/10.2118/27969-MS

de Beer, J., Price, S.J., & Ford, J.R. (2012a). 3D modelling of geological and anthropogenic deposits at the World Heritage Site of Bryggen in Bergen, Norway. *Quaternary Intenational*, *251*, 107-116. https://doi.org/10.1016/j.quaint.2011.06.015

de Beer, J., Matthiesen, H., & Christensson, A. (2012b). Quantification and visualization of in situ degradation at the World Heritage Site Bryggen in Bergen, Norway. *Conservation and Management of Archaeological Sites*, *14*(1-4), 215-227. https://doi.org/10.1179/1350503312Z.00000000018

De Rienzo, F., Oreste, P., & Pelizza, S. (2008). Subsurface geological-geotechnical modelling to sustain underground civil planning. *Engineering Geology*, *96*(3-4), 187-204. https://doi.org/10.1016/j.enggeo.2007.1l.002

Gallerini, G., & De Donatis, M. (2009). 3D modelling using geognostic data: The case of the low valley of Foglia river (Italy). *Computers and Geosciences*, *35*(1), 146-164. https://doi.org/10.1016/j.cageo.2007.09.012

Ghiglieri, G., Carletti, A., Da Pelo, S., Cocco, F., Funedda, A., Loi, A., Manta, F., & Pittalis, D. (2016). Three-dimensional hydrogeological reconstruction based on geological depositional model: a case study from the coastal plain of Arborea (Sardinia, Italy). *Engineering Geology*, *207*, 103-114. https://doi.org/10.1016/j.enggeo.2016.04.014

Kaufmann, O., & Martin, T. (2009). 3D geological modelling from boreholes, cross-sections and geological maps, application over former natural gas storages in coal mines. *Computers and Geosciences*, *35*(1), 70-82.

https://doi.org/10.1016/S0098-3004(08)00227-6

Kessler, H., Mathers, S., & Sobisch, H.G. (2009). The capture and dissemination of integrated 3D geospatial knowledge at the British Geological Survey using GSI3D software and methodology. *Computers and Geosciences*, *35*(6), 1311-1321. https://doi.org/10.1016/j.cageo.2008.04.005

Lemon, A.M., & Jones, N.L. (2003). Building solid models from boreholes and user-defined cross-sections. *Computers and Geosceinces, 29*(5), 547-555. https://doi.org/10.1016/S0098-3004(03)00051-7

Manual, T. (2013). Solid Model Algorithms. RockWare, Golden.

Ming, J., Pan, M., Qu, H., Ge, Z. (2010). GSIS: A 3D geological multi-body modelling system from netty cross-sections with topology. *Computers and Geosciences*, *36*(6), 756-767. https://doi.org/10.1016/j.cageo.2009.11.003

Royse, K.R., Rutter, H.K., & Entwisle, D.C. (2009). Property attribution of 3D geological models in the Thames Gateway, London: new ways of visualising geoscientific information. Bulletin of *Engineering Geology and the Environment*, *68*(1), 1-16. https://doi.org/10.1007/s10064-008-0171-0

Sheikh, I.M., Pasha, M.K., Williams, V.S., Raza, S.Q., & Khan, K.S. (2008). Environmental geology of the Islamabad-Rawalpindi area, northern Pakistan. Chapter G of "Regional Studies of the Potwar-Plateau Area, Northern Pakistan"; Warwick, P.D., & Wardlaw, B.R. (Eds.). U.S. Department of the Interior, U.S. Geological Survey Bulletin 2078-G.

Staveren, M.T.V., & Knoeff, J.G. (2004). The geotechnical baseline report as risk allocation tool. In *Engineering Geology for Infrastructure Planning in Europe* (pp. 777-785). Springer, Berlin, Heidelberg. https://doi.org/10.1007/978-3-540-39918-6_86

Tame, C., Cundy, A.B., Royse, K.R., Smith, M., & Moles, N.R. (2013). Three-dimensional geological modelling of anthropogenic

deposits at small urban sites: a case study from Sheepcote Valley, Brighton, UK. *Journal of Environmental Management*, *129*, 628-634. https://doi.org/10.1016/j.jenvman.20 2013.08.030

Touch, S., Likitlersuang, S., & Pipatpongsa, T. (2014). 3D geological modelling and geotechnical characteristics of Phnom Penh subsoils in Cambodia. *Engineering Geology*, *178*, 58-69. https://doi.org/10.1 106/j.enggeo.2014.06.010

Turner, A.K. (2003). Definition of the modelling technologies. In *New paradigms in subsurface prediction* (pp. 27-40). Springer, Berlin, Heidelberg. https://doi.org/10.1007/3-540-48019-63

Viseur, S., & Shtuka, A. (1997). Advances in stochastic boolean simulation of channels. In *15th GOCAD Meeting Report*.

Zhu, L., Zhang, C., Li, M., Pan, X., & Sun, J. (2012). Building 3D solid models of sedimentary stratigraphic systems from borehole data: an automatic method and case studies. *Engineering Geoogy*, *127*, 1-13.https://doi.org/10.1016/j.enggeo.2011.12.001

LOCATION DATA SHEET (APPENDIX A)
Bore	**Easting**	**Northing**	**Elevation**	**TD (m)**	**Bore**	**Easting**	**Northing**	**Elevation**	**TD (m)**
BH-01	290643.0329	3736240.016	452.0184	7.62	**BH-30**	288377.6	3735689	448.6656	7.62
BH-02	291072.2217	3736325.376	458.724	7.62	**BH-31**	288387.1	3735549	447.7512	7.62
BH-03	290969.7635	3736518.691	454.7616	7.62	**BH-32**	288062.4	3735371	454.7616	7.62
BH-04	290761.6006	3736583.169	460.8576	7.62	**BH-33**	288247.9	3735012	454.152	7.62
BH-05	288776.4936	3735702.457	462.9912	7.62	**BH-34**	288430.9	3735406	447.7512	7.62
BH-06	290443.4569	3736581.935	457.5048	7.62	**BH-35**	288173.6	3735373	451.4088	7.62
BH-07	290326.3769	3736336.62	455.3712	7.62	**BH-36**	288698.3	3734903	439.8264	7.62
BH-08	290411.6384	3736635.672	458.1144	7.62	**BH-37**	288911.2	3734822	452.0184	7.62
BH-09	290440.8759	3736291.165	452.9328	7.62	**BH-38**	288783.2	3734874	450.4944	7.62
BH-10	290512.4048	3736112.281	455.0664	7.62	**BH-39**	288608.2	3735260	442.8744	7.62
BH-11	290521.3351	3736029.198	456.2856	7.62	**BH-40**	289293.8	3735569	454.152	7.62
BH-12	289909.1582	3736100.567	447.7512	7.62	**BH-41**	289281.7	3734792	451.104	7.62
BH-13	289851.5406	3735571.554	451.7136	7.62	**BH-42**	289304.2	3735526	455.3712	7.62
BH-14	289727.8059	3735618.884	452.9328	7.62	**BH-43**	289386	3735519	456.2856	7.62
BH-15	289548.0886	3735767.535	450.7992	7.62	**BH-44**	288692.8	3734691	448.3608	7.62
BH-16	288816.7118	3736125.218	445.6176	7.62	**BH-45**	288904.5	3736344	461.772	7.62
BH-17	288676.8569	3736151.503	446.532	7.62	**BH-46**	289445	3734124	463.296	7.62
BH-18	288541.347	3736281.887	442.8744	7.62	**BH-47**	288657.5	3734579	454.152	7.62
BH-19	288708.387	3735707.958	454.152	7.62	**BH-48**	288775.8	3734500	454.7616	7.62
BH-20	288655.4601	3735670.514	449.58	7.62	**BH-49**	288795	3734177	457.8096	7.62
BH-21	288779.2299	3735687.86	454.7616	7.62	**BH-50**	289384.8	3734412	454.4568	7.62
BH-22	288676.9935	3735897.953	449.58	7.62	**BH-51**	289980.6	3734246	465.4296	7.62
BH-23	288761.1788	3735500.402	456.8952	7.62	**BH-52**	290355.8	3733494	463.9056	7.62
BH-24	288636.3385	3735836.936	448.9704	7.62	**BH-53**	290048	3733843	455.9808	7.62
BH-25	288301.4573	3736102.451	447.4464	7.62	**BH-54**	290201.3	3733496	469.392	7.62
BH-26	288319.6108	3735604.051	449.2752	7.62	**BH-55**	291519.9	3733551	476.0976	7.62
BH-27	288138.8121	3735991.434	450.4944	7.62	**BH-56**	291311	3733371	478.2312	7.62
BH-28	288246.1521	3736083.149	448.6656	7.62	**BH-57**	291325.2	3733444	477.012	7.62
BH-29	288036.7423	3735585.913	453.2376	7.62	**BH-58**	289033.6	3735715	453.5424	7.62

LITHOLOGY TYPE DATA SHEET (APPENDIX B)
Name	**Pattern**	**Size**	**Background**	**Foreground**	**Thickness**	**Percent**	**Density**	**G-Value**
SC - 1	5	2	16752190	0	1	100	1	1
SC - 2	10	2	8454143	255	2	100	1	2
SC - 3	15	2	16711808	16777215	3	100	1	3

LITHOLOGY DATA SHEET (APPENDIX C)											
Borehole	Depth To Top	Depth to Bottom	Lithology	Borehole	Depth To Top	Depth to Bottom	Lithology	Borehole	Depth To Top	Depth to Bottom	Lithology
BH-01	0	2.4384	SC - 1	BH-21	2.7432	5.7912	SC - 2	BH-42	0	3.048	SC - 1
BH-01	2.4384	5.7912	SC - 2	BH-21	5.7912	7.62	SC - 3	BH-42	3.048	5.1816	SC - 2
BH-01	5.7912	7.62	SC - 3	BH-22	0	2.1336	SC - 1	BH-42	5.1816	7.62	SC - 3
BH-02	0	3.6576	SC - 1	BH-22	2.1336	6.7056	SC - 2	BH-43	0	3.3528	SC - 1
BH-02	3.6576	7.62	SC - 2	BH-22	6.7056	7.62	SC - 3	BH-43	3.3528	6.096	SC - 2
BH-03	0	3.048	SC - 1	BH-23	0	4.572	SC - 1	BH-43	6.096	7.62	SC - 3
BH-03	3.048	7.62	SC - 2	BH-23	4.572	7.62	SC - 2	BH-44	0	1.524	SC - 1
BH-04	0	0.9144	SC - 1	BH-24	0	1.524	SC - 1	BH-44	1.524	3.048	SC - 2
BH-04	0.9144	5.4864	SC - 2	BH-24	1.524	5.1816	SC - 2	BH-44	3.048	7.62	SC - 3
BH-04	5.4864	7.62	SC - 3	BH-24	5.1816	7.62	SC - 3	BH-45	0	1.524	SC - 1
BH-05	0	2.7432	SC - 1	BH-25	0	2.1336	SC - 1	BH-45	1.524	6.096	SC - 2
BH-05	2.7432	3.9624	SC - 2	BH-25	2.1336	3.9624	SC - 2	BH-45	6.096	7.62	SC - 3
BH-05	3.9624	7.62	SC - 3	BH-25	3.9624	7.62	SC - 3	BH-46	0	0.6096	SC - 1
BH-06	0	2.4384	SC - 1	BH-26	0	3.9624	SC - 1	BH-46	0.6096	4.572	SC - 2
BH-06	2.4384	6.096	SC - 2	BH-26	3.9624	7.62	SC - 2	BH-46	4.572	7.62	SC - 3
BH-06	6.096	7.62	SC - 3	BH-27	0	1.2192	SC - 1	BH-47	0	2.1336	SC - 1
BH-07	0	1.8288	SC - 1	BH-27	1.2192	4.2672	SC - 2	BH-47	2.1336	6.096	SC - 2
BH-07	1.8288	5.4864	SC - 2	BH-27	4.2672	7.62	SC - 3	BH-47	6.096	7.62	SC - 3
BH-07	5.4864	7.62	SC - 3	BH-28	0	1.8288	SC - 1	BH-48	0	3.048	SC - 1
BH-08	0	1.524	SC - 1	BH-28	1.8288	3.6576	SC - 2	BH-48	3.048	6.096	SC - 2
BH-08	1.524	3.6576	SC - 2	BH-28	3.6576	7.62	SC - 3	BH-48	6.096	7.62	SC - 3
BH-08	3.6576	7.62	SC - 3	BH-29	0	0.9144	SC - 1	BH-49	0	1.524	SC - 1
BH-09	0	1.524	SC - 1	BH-29	0.9144	6.096	SC - 2	BH-49	1.524	7.62	SC - 2
BH-09	1.524	3.3528	SC - 2	BH-29	6.096	7.62	SC - 3	BH-50	0	0.9144	SC - 1
BH-09	3.3528	7.62	SC - 3	BH-30	0	0.9144	SC - 1	BH-50	0.9144	4.2672	SC - 2
BH-10	0	2.1336	SC - 1	BH-30	0.9144	7.62	SC - 2	BH-50	4.2672	7.62	SC - 3
BH-10	2.1336	3.3528	SC - 2	BH-31	0	3.6576	SC - 1	BH-51	0	0.6096	SC - 1
BH-10	3.3528	7.62	SC - 3	BH-31	3.6576	7.62	SC - 2	BH-51	0.6096	4.8768	SC - 2
BH-11	0	0.9144	SC - 1	BH-32	0	0.6096	SC - 1	BH-51	4.8768	7.62	SC - 3
BH-11	0.9144	6.096	SC - 2	BH-32	0.6096	5.4864	SC - 2	BH-52	0	2.4384	SC - 1
BH-11	6.096	7.62	SC - 3	BH-32	5.4864	7.62	SC - 3	BH-52	2.4384	5.1816	SC - 2
BH-12	0	0.9144	SC - 1	BH-33	0	2.4384	SC - 1	BH-52	5.1816	7.62	SC - 3
BH-12	0.9144	6.096	SC - 2	BH-33	2.4384	5.4864	SC - 2	BH-53	0	3.6576	SC - 1
BH-12	6.096	7.62	SC - 3	BH-33	5.4864	7.62	SC - 3	BH-53	3.6576	6.4008	SC - 2
BH-13	0	1.524	SC - 1	BH-34	0	0.9144	SC - 1	BH-53	6.4008	7.62	SC - 3
BH-13	1.524	3.048	SC - 2	BH-34	0.9144	5.1816	SC - 2	BH-54	0	1.8288	SC - 1
BH-13	3.048	7.62	SC - 3	BH-34	5.1816	7.62	SC - 3	BH-54	1.8288	7.62	SC - 2
BH-14	0	4.572	SC - 1	BH-35	0	3.6576	SC - 1	BH-55	0	0.6096	SC - 1
BH-14	4.572	7.62	SC - 2	BH-35	3.6576	7.62	SC - 2	BH-55	0.6096	4.572	SC - 2
BH-15	0	1.524	SC - 1	BH-36	0	2.1336	SC - 1	BH-55	4.572	7.62	SC - 3
BH-15	1.524	4.572	SC - 2	BH-36	2.1336	6.7056	SC - 2	BH-56	0	1.524	SC - 1
BH-15	4.572	7.62	SC - 3	BH-36	6.7056	7.62	SC - 3	BH-56	1.524	2.4384	SC - 2
BH-16	0	0.9144	SC - 1	BH-37	0	0.9144	SC - 1	BH-56	2.4384	7.62	SC - 3
BH-16	0.9144	6.4008	SC - 2	BH-37	0.9144	4.572	SC - 2	BH-57	0	1.524	SC - 1
BH-16	6.4008	7.62	SC - 3	BH-37	4.572	7.62	SC - 3	BH-57	1.524	6.4008	SC - 2
BH-17	0	3.6576	SC - 1	BH-38	0	3.048	SC - 1	BH-57	6.4008	7.62	SC - 3
BH-17	3.6576	7.62	SC - 2	BH-38	3.048	6.096	SC - 2	BH-58	0	0.9144	SC - 1
BH-18	0	1.524	SC - 1	BH-38	6.096	7.62	SC - 3	BH-58	0.9144	4.8768	SC - 2
BH-18	1.524	7.62	SC - 2	BH-39	0	1.524	SC - 1	BH-58	4.8768	7.62	SC - 3
BH-19	0	1.8288	SC - 1	BH-39	1.524	7.62	SC - 2				
BH-19	1.8288	4.572	SC - 2	BH-40	0	0.9144	SC - 1				
BH-19	4.572	7.62	SC - 3	BH-40	0.9144	4.2672	SC - 2				
BH-20	0	3.048	SC - 1	BH-40	4.2672	7.62	SC - 3				
BH-20	3.048	6.7056	SC - 2	BH-41	0	1.2192	SC - 1				
BH-20	6.7056	7.62	SC - 3	BH-41	1.2192	6.096	SC - 2				
BH-21	0	2.7432	SC - 1	BH-41	6.096	7.62	SC - 3				